Gasochromic WO$_3$ Nanostructures for the Detection of Hydrogen Gas: An Overview

Ali Mirzaei [1],*, Jae-Hun Kim [2], Hyoun Woo Kim [3,4],* and Sang Sub Kim [2],*

[1] Department of Materials Science and Engineering, Shiraz University of Technology, Shiraz 71557-13876, Iran
[2] Department of Materials Science and Engineering, Inha University, Incheon 22212, Korea;
    kjhhb5331@gmail.com
[3] The Research Institute of Industrial Science, Hanyang University, Seoul 04763, Korea
[4] Division of Materials Science and Engineering, Hanyang University, Seoul 04763, Korea
* Correspondence: mirzaei@sutech.ac.ir (A.M.); hyounwoo@hanyang.ac.kr (H.W.K.);
    sangsub@inha.ac.kr (S.S.K.)

check for updates

Abstract: Hydrogen is one of the most important gases that can potentially replace fossil fuels in the future. Nevertheless, it is highly explosive, and its leakage should be detected by reliable gas sensors for safe operation during storage and usage. Most hydrogen gas sensors operate at high temperatures, which introduces the risk of hydrogen explosion. Gasochromic WO$_3$ sensors work based on changes in their optical properties and color variation when exposed to hydrogen gas. They can work at low or room temperatures and, therefore, are good candidates for the detection of hydrogen leakage with low risk of explosion. Once their morphology and chemical composition are carefully designed, they can be used for the realization of sensitive, selective, low-cost, and flexible hydrogen sensors. In this review, for the first time, we discuss different aspects of gasochromic WO$_3$ gas sensor-based hydrogen detection. Pristine, heterojunction, and noble metal-decorated WO$_3$ nanostructures are discussed for the detection of hydrogen gas in terms of changes in their optical properties or visible color. This review is expected to provide a good background for research work in the field of gas sensors.

Keywords: gasochromic; nanostructured WO$_3$; gas sensor; hydrogen gas; sensing mechanism

1. Hydrogen Gas

Hydrogen is a gas with no color, odor, or taste and cannot be detected by human senses [1,2]. Due to its efficiency, renewability, and green nature, it can replace fossil fuels in the near future [3]. Nevertheless, because of its small size, high diffusion coefficient, and consequently easy permeation through most materials, it is difficult to store hydrogen. Furthermore, hydrogen is highly explosive with a broad flammability range (4–75 vol%) and possesses an extremely low ignition energy [4,5]. Therefore, it is important to develop reliable and safe gas sensors for detecting hydrogen gas. So far, several gas sensors based on different mechanisms have been reported for sensing hydrogen, including fiber-optic [6], catalytic [7], electrochemical [8], acoustic [9], resistive [10], thermoelectric [11], and gasochromic gas sensors [12]. Each of these sensors has its own merits and shortages [13]. For example, resistive gas sensors are inexpensive, simple in design and operation, highly responsive, and exhibit good stability [14–16]. However, they can only work efficiently at high temperatures [17], which increases the risk of hydrogen explosion during detection. Gasochromic sensors have the advantage of working at low temperatures, which can significantly decrease the risk of hydrogen explosion. Furthermore, in some cases, they can be fabricated on flexible substrates, with eye-readable color changes, which remarkably facilitate the detection of hydrogen in different places. In addition, the removal of electrical power from ambient atmosphere, high resistance to electromagnetic noise, and

compatibility with optical fibers make them advantageous in hydrogen gas detection [18]. In this review, we will focus on gasochromic gas sensors based on WO_3. First, we introduce one of the most widely-used materials for fabricating gasochromic sensors, i.e., WO_3, after which we discuss different gasochromic WO_3 gas sensors.

2. WO_3 and Its Crystal Structure

Tungsten trioxide (WO_3) is a very promising metal oxide with diverse properties. It has an n-type (E_g = 2.60–3.25 eV) [19,20] semiconducting nature and unique electrical properties. Further, it is transparent to visible and infrared light. Therefore, it has been used in different applications including smart windows [21], photocatalysts [22], solar cells [23], humidity sensors [24], and gas sensors [25]. Moreover, due to its excellent coloration efficiency [26], WO_3 is the most used chromogenic material in photochromic, electrochromic, and gasochromic applications [27].

Tungsten oxide has a perovskite-type WO_6 octahedral crystal structure (Figure 1). In its structure, W^{6+} ions occupy the corners of the octahedra, and oxygen ions are located at mid-crystal edge. In the ideal form, the octahedra are connected at the corners. The central atom (C) is absent and this defective perovskite configuration is often referred to as the ReO_3 structure [28].
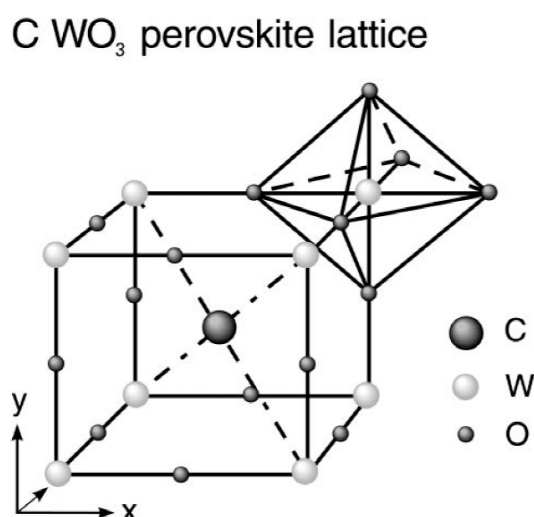
Figure 1. The perovskite lattice of WO_3 (Reprinted with permission from [28]).

Similar to the behavior of most perovskites and ceramics, depending on the temperature, WO_3 crystals can structurally transform in the following order: Monoclinic (ε-WO_3, <−43 °C), triclinic (δ-WO_3, −43 to 17 °C), monoclinic (γ-WO_3, 17–330 °C), orthorhombic (β-WO_3, 330–740 °C), and tetragonal (α-WO_3 > 740 °C) [29,30]. The monoclinic crystal structure is the most stable at room temperature [30]. The large voids generated in WO_6 octahedral networks in the WO_3 structure induce some variations in the position of W and in the WO_6 octahedron orientation. Thus, displacement of tungsten from the center of the octahedron and tilting of the WO_6 octahedra are two kinds of distortions [26], which lead to 11 different structures of WO_3 [31]. The gasochromic coloration of crystalline WO_3 is associated with changes in its structure from monoclinic to tetragonal and cubic [32]. For example, Inouye et al. [33] reported crystal structure transition from monoclinic to tetragonal in RF-sputtered WO_3 films upon exposure to hydrogen gas. However, the structure of hydrated $WO_3 \cdot xH_2O$ sensors does not change during gasochromic detection of hydrogen gas [32].

3. Chromogenic: Definition, Materials and Basics

Chromogenics is a Greek word with the stem "chromo" for color. It refers to the study of materials whose optical properties (color) change as a function of external ambient conditions [31]. Chromogenic materials generally have wide bandgaps and are transparent in the visible range,

but they reversibly change from being transparent to a dark color in the presence of an electric field (electrochromic coloration), light (photochromic coloration), or when they are exposed to a gas (gasochromic coloration) [34]. Therefore, gasochromism refers to reversible changes in optical properties or color when a material is exposed to a gas [3,35]. Gasochromic materials exhibit a promising potential for use as gas sensors. WO_3, which is light yellow in color, is one of the most important chromogenic materials known thus far. It exhibits a deep blue color upon exposure to hydrogen gas [36]. In addition to WO_3, other materials reported for gasochromic applications include V_2O_5 [37–40], VO_x [41], MO_x [42], MoO_3 [43], $(MoO_3)_{1-x}$ $(V_2O_5)_x$ [44], mixed silver/nickel ammonium phosphomolybdate [45], $(Ti-V-Ta)O_x$ [35], $Ni(OH)_2$ [46], peroxopolytungstic acid [47,48], and metals like Y [49]. This effect has also been exploited for the detection of other gases such as volatile organic compounds [50], NO_2 [51], H_2S, SO_2 [52], NH_3 [53], XeF_2 [54], cyclohexane [55], CO, and Cl_2 [46]. Among the different gasochromic materials available, the most important ones are WO_3 and MoO_x. However, due to its weak color change properties and the existence of several phases whose formation depends on the growth method, molybdenum oxide has received less attention for gasochromic studies [56].

The ability of WO_3 to undergo reversible changes in its optical properties when exposed to an electric field was first reported by Deb in 1973 [57]. Nineteen years later, Ito [58] reported the potential of WO_3 for gasochromic studies. Thus far, the optical properties of WO_3 nanostructures have been modulated by applying an electric field (electrochromism), UV irradiation (photochromism), or a gas (gasochromism) [59]. Gasochromic coloration of WO_3 is mostly associated with hydrogen gas [35]. In contrast to the electrochromic response, the presence of catalytic noble metals on the surfaces of WO_3 nanostructures is necessary to induce an acceptable gasochromic effect. The most common catalysts used are Pd [60,61], Au [30], and Pt [62,63]. They promote chemical reactions by reducing the activation energy between WO_3 and hydrogen gas. Color changes occur in gasochromic WO_3 sensors when H^+ ions intercalate with the WO_3 layer after the dissociation of gas molecules (H_2) into atoms by the action of noble metals. The optical properties of WO_3 films can be reversibly changed with the insertion and extraction of H^+ ions and electrons into the WO_3 films, which is accompanied by redox changes leading to the formation of W^{5+} ions [64,65]. Gasochromic measurements are often carried out by monitoring optical properties, such as absorbance/transmittance/reflectance in convenient wavelength ranges (visible-NIR) [66]. Such measurements offer simple, low-cost, and highly selective analytical methods for detecting specific gases [30]. In addition, the stability of the gas sensor can be enhanced as measurements are most often conducted at low or room temperatures.

3.1. General Sensing Mechanism of Gasochromic WO_3

Currently, there are four models related to the gasochromic coloration of WO_3 sensors, namely charge transfer of electrons between (i) W^{6+}/W^{5+} states, (ii) W^{5+}/W^{4+} states, (iii) W^{6+}/W^{5+} and W^{5+}/W^{4+} states, and (iv) the oxygen vacancy model. In the first three models, the gasochromic coloration of WO_3 is explained by charge transfer-electron transitions between different states and the composition of the colored state changes to tungsten bronze (H_xWO_3) due to the double injection of hydrogen ions and electrons into WO_3 lattice as follows [67]:

$$xH^+ + xe^- + WO_3 \rightarrow H_xWO_3 \tag{1}$$

The above reaction is comprised of following steps (i) absorption and dissociation of the H_2 on the surface of noble metal, (ii) spillover of the H from the noble metal onto the WO_3 surface, (iii) diffusion of H along the grain surface of WO_3, (iv) injection of H into the outer surfaces of WO_3, (v) diffusion of H into the interior of WO_3 lattice and formation of H_xWO_3 [68]. The magnitude of coloration in H_xWO_3 is closely related to the amount of hydrogen insertion (*x*), which usually varies with the structure, morphology, and crystallinity of the WO_3 sensing layer [67,69]. The oxygen vacancy model supposes the formation of a sub-stoichiometric WO_{3-x} structure due to the formation of oxygen vacancies [67].

In fact, in the oxygen vacancy model, H_2 is dissociated on the noble metal and then transferred to WO_3, where it reacts with oxygen on the surface of WO_3, leading to the formation of water and oxygen vacancies and a blue color as follows [70]:

$$xH^+ + xe^- + WO_3 \rightarrow H_xWO_3 \tag{2}$$

The oxygen vacancies diffuse into the interior of the WO_3 and lead to the coloration, while the H_2O slowly desorbs from the WO_3 [68].

A challenging task in gasochromic sensor science lies in improving sensor dynamics, which is important for the rapid detection of hydrogen leakage. Reduction of sensor size from micro to nano-scale increases its surface area significantly, which means an increase in the number of available surface sites for the adsorption of atomic hydrogen, leading to faster sensor dynamics. Furthermore, nanostructured gas sensors are expected to exhibit an improved response to H_2 gas even at low concentrations [30]. In the following sections, different WO_3 nanostructured gasochromic sensors are presented and discussed.

3.2. Gasochromic WO_3 Nanostructures as Hydrogen Gas Sensors

Generally, substrate temperature affects the crystallinity and morphology of as-grown films, which eventually leads to differences in their gasochromic coloration. Yamamoto et al. [71] studied the gasochromic performance of epitaxial WO_3 sensors deposited by pulsed laser deposition (PLD) at different substrate temperatures. Changes in the optical density (OD) of the WO_3 sensor at $\lambda = 645$ nm between the initial and colored states when exposed to 1% H_2/Ar for 20 min, i.e., optical density (ΔOD) $= -\log(T_{colored}/T_{initial})$, were obtained. The ΔOD of the film deposited at 432 °C rapidly changed when exposed to hydrogen gas. With an increase in the substrate temperature, the coloration reduced, and in the film deposited at 538 °C (with better crystallinity), almost no coloration was observed. This was in contrast to previous reports on the enhancement in gasochromic coloration due to structural changes, where highly crystalline WO_3 nanowires (NW) films with a monoclinic structure transformed into the tetragonal phase upon hydrogen gasochromic coloration. Thus, the researchers highlighted that controlling the free space between WO_3 grains for the relaxation of mechanical stresses during structural transformation is essential when a sensor is exposed to hydrogen gas.

Behbahani et al. [72] prepared WO_3/glass thin film gas sensors by PLD at various substrate temperatures (25–400 °C) for the gasochromic investigation of hydrogen. Figure 2a shows images of different colors the gas sensors exhibited at various substrate temperatures.

Coloring was initiated from the boundary edge of the $PdCl_2$ drop as a tiny blue ring and gradually extended to the center, suggesting that hydrogen initially entered at the triple points of the substrate, liquid, and gas. In hydrogen atmosphere, Pd nanoparticles (NPs) were produced over the surface as well as at the triple points. The formation of Pd was accompanied by the gasochromic coloring of tungsten oxide. Hydrogen, with its reducing power, helps the accumulation of a layer of Pd NPs, as shown in Figure 2b. In the samples deposited at temperatures below 200 °C, a uniform coloring was observed. At 200 °C, a very deep blue color was obtained due to the high surface porosity of the sensor film. However, the uniformity of coloring decreased significantly with an increase in the deposition temperature.

Pd, Pt, and Au catalysts are known to be highly reactive to activation by hydrogen, and they are often used along with WO_3 to increase gasochromic efficiency by the dissociation of hydrogen atoms. Garavand et al. [73] prepared Pt/WO_3 and Pd/WO_3 films by PLD and studied the effect of operating temperature (30–200 °C) on their gasochromic properties. Coloration was evaluated by measuring the optical density (ΔOD) at $\lambda = 632.8$ nm as follows,

$$\Delta OD = -\ln\left(\frac{I(t)}{I(t_0)}\right) \tag{3}$$

where $I(t)$ and $I(t_0)$ represent the optical transmission intensities of the colored and bleached states, respectively. Pristine WO_3 did not show any noticeable response to hydrogen gas, while, due to the spillover effect of Pt, Pt/WO_3 films showed a good response to hydrogen gas. The response of the Pt/WO_3 sensor was almost constant in the range of 85–200 °C. At lower temperatures, its response was negligible, and its dynamics were slow due to the slow dissociation of hydrogen gas and low diffusivity of the hydrogen atoms. At 200 °C, the effect of humidity on the gas response was negligible. Further, the risk of catalyst poisoning with contaminants was lower at this temperature when compared to those at lesser temperatures. Therefore, this temperature was reported to be the optimal sensing temperature. In addition, the higher response of the Pt/WO_3 sensor when compared to that of the Pd/WO_3 sensor was attributed to the hydrogen spillover effect of Pt and Pd. As the dissolution rate of hydrogen in Pd is higher than that in Pt, the spillover range of hydrogen on the Pt surface is longer. Therefore, the number of injected species into the WO_3 lattice in Pt/WO_3 was higher than that in Pd/WO_3. This implies that in the Pt/WO_3 gas sensor, more color centers were activated, leading to a higher gasochromic response. In contrast, the Pd-WO_3 gas sensor was capable of detecting H_2 gas at lower temperatures [73].
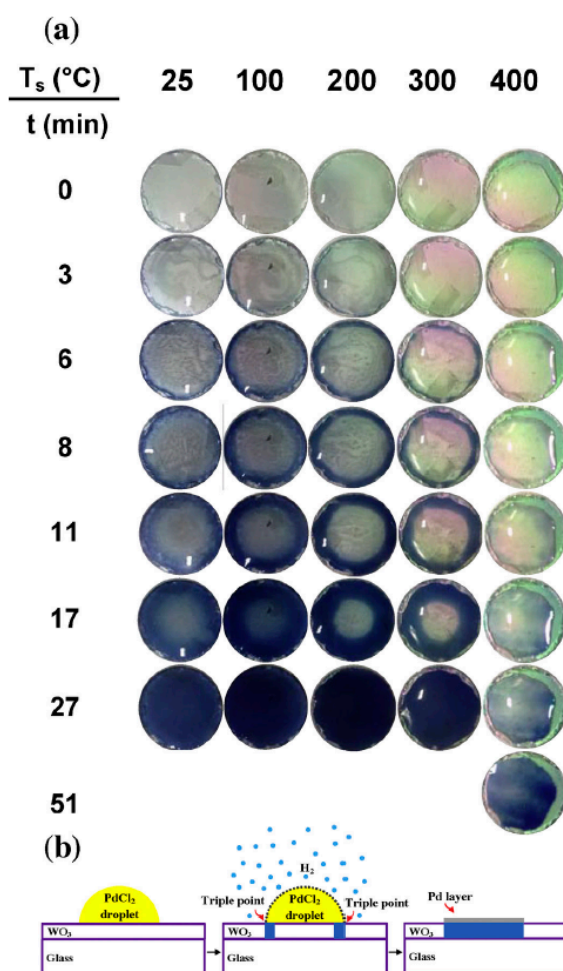

Figure 2. (a) Photographs of coloration of $PdCl_2(aq)/WO_3/glass$ sensors deposited at different temperatures and exposed to hydrogen gas; (b) An illustration of the gasochromic coloration effect. (Reprinted with permission from [72]).

Lee et al. [74] investigated the gasochromic mechanism of amorphous Pd/WO_3 films using Raman scattering tests. Firstly, when a Pd/WO_3 gas sensor was exposed to hydrogen, hydrogen dissociation occurred on the Pd surface, and these atoms diffused across the Pd layer. Subsequently, atomic hydrogen and electrons were inserted at the Pd/WO_3 interface. Later, W^{6+} ions were reduced to W^{5+}

by procuring one electron from the hydrogen atom, resulting in a change in the color of WO_3. For gasochromic bleaching in the presence of oxygen, there occurred a recombination reaction between atomic hydrogen (on Pd) and oxygen gas, leading to the formation of water molecules and oxidation of W^{5+} to W^{6+}.

In another study related to amorphous WO_3 films, Lee et al. [75] deposited amorphous WO_3 thin films with thicknesses of 270, 540, and 760 nm by RF sputtering, and subsequently Pd nanoparticles (NPs) layers of different thicknesses (<5 nm) were deposited by e-beam evaporation. Figure 3 shows a schematic of the developed gas sensing system. To quantitatively measure visible color changes in the Pd-WO_3 sensor, measurements were carried out in the wavelength range of 300 to 1100 nm at room temperature.
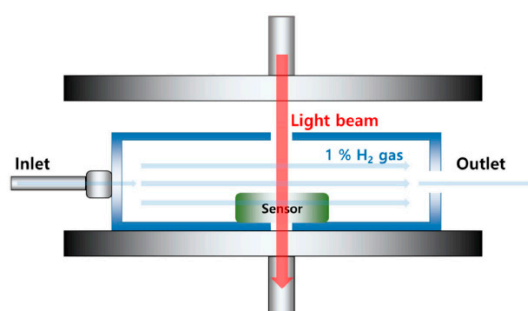

Figure 3. In situ gasochromic sensing by UV-Vis transmittance. (Reprinted with permission from [75]).

The optimal thickness of Pd on WO_3 films was found to be 3–4 nm. The transmittance spectrum obtained after exposure to 1% H_2 gas for 10 min showed a 50% difference in the transmittance before and after exposure to H_2 gas. The influence of temperature on coloration was investigated in the range of 298 to 473 K. Transmittance was found to increase with an increase in temperature. Color degradation occurred due to annealing, where grain growth led to a decrease in the grain boundary diffusion of protons. Furthermore, surface water molecules, which provided channels for oxygen vacancies, evaporated, and the evacuated cavities were covered with some oxygen.

Color difference measurements showed that a thick gas sensor provided better coloration difference. The structure of the thinnest WO_3 film was dense, while, at higher thicknesses, the films exhibited a porous structure. Further, different gas compositions, including pure H_2 (10 sccm), H_2 + CH_4 (5:5 sccm), pure CH_4 (10 sccm), and H_2 + CO (5:5 sccm), were tested (Figure 4a). Pure CH_4 gas did not result in any changes in transmittance, while H_2 + CO resulted in a slightly decreased transmittance due to Pd poisoning by CO gas. On the other hand, the H_2 + CH_4 mixture showed the lowest transmittance and greatest coloration. Enhanced coloration with the H_2 + CH_4 mixture may be related to the oxidation of CH_4 on Pd, which produced CH_3OH and H_2O. As a result, additional hydrogen atoms were produced. They diffused into the WO_3 lattice, reacted to form an intermediate W=O-H state, and produced H_2O, thereby creating oxygen vacancies. Consequently, the amount of W^{5+} sites inducing coloration increased. A Pd-WO_3 flexible gas sensor was also prepared on a polyester substrate (Figure 4b,c). No annealing was performed during the fabrication of the flexible gas sensor. The sensor exhibited coloration without cracks or failure upon bending, which is important for some applications. For example, joints in supply lines are potential leakage points for hydrogen gas. A flexible and bendable sensor can conform to the morphology of the joint. Accordingly, low cost and flexible gasochromic H_2 sensors can facilitate H_2 detection at leakage sites with unusual shapes.

In another study related to the thickness of the sensing film, Shanak et al. [76] deposited WO_3 thin films with different thicknesses in a mixed atmosphere of O_2 and Ar gas using a reactive DC-sputtering technique. Subsequently, Pt was deposited using a sputtering method—films of different thicknesses showed different response times. Thin films (20–170 nm) exhibited long coloring and bleaching times between coloration and bleaching states. Thicker films showed shorter switching times. The

shortest switching time was found for the thickest sample (~1000 nm) with a coloration rate of 1.64%/s. Additionally, the thickest film showed good saturation, reversibility, and stability.
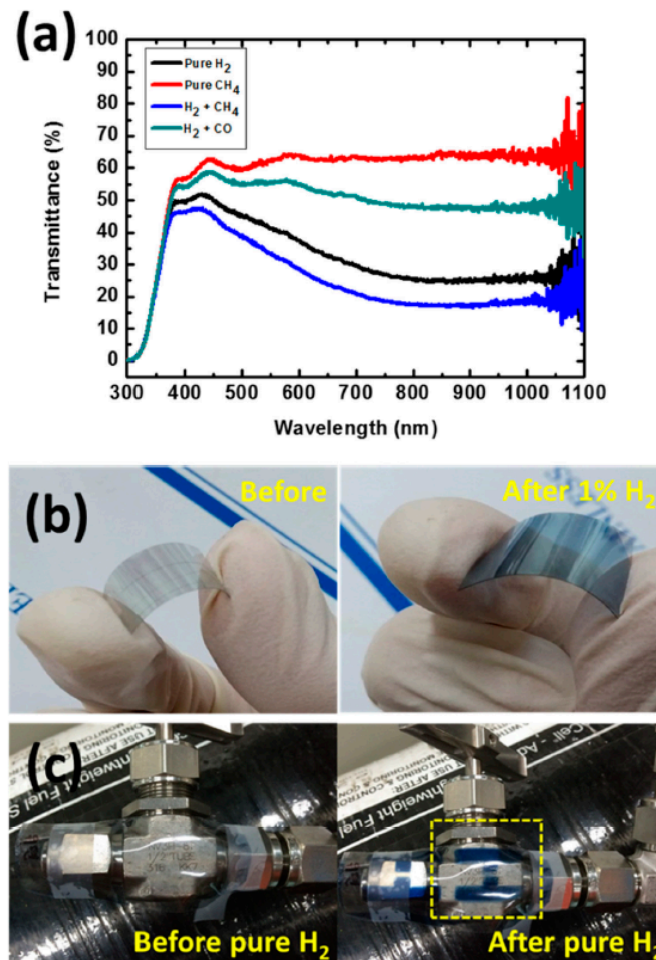
Figure 4. (**a**) Transmittance spectra in the presence of various gases; (**b**) Digital images of flexible Pd-WO$_3$ sensors before and after exposure to 1% H$_2$; (**c**) A gasochromic flexible Pd-WO$_3$ sensor on a gas pipeline carrying pure H$_2$. (Reprinted with permission from [75]).

In their investigation, Nishizawa et al. [77] fabricated WO$_3$ amorphous films decorated with Pt using UV irradiation. Changes in the optical transmittance of the films were studied by measuring the light intensity of a laser ($\lambda = 670$ nm) with a silicon photodiode (Figure 5).
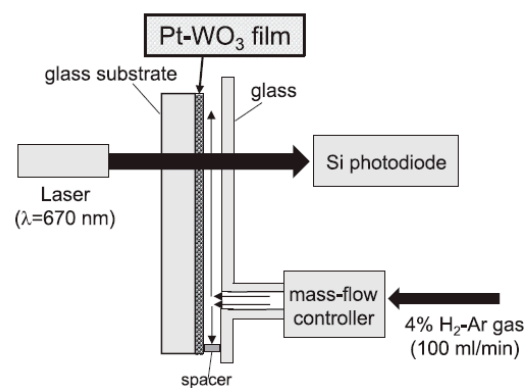
Figure 5. H$_2$ gas switching system for Pt-WO$_3$ films. (Reprinted with permission from [77]).

The optical transmittance of Pt-WO$_3$ sensors at λ = 670 nm was measured as a function of time during exposure to a 60 s cycle of hydrogen injection and removal. Optical changes in the presence of H$_2$ gas or air were quite large (~70%). In the case of the gas sensor with a film thickness of 400 nm, the response time was small (~5 s), while a thicker film required more time due to the slow diffusion of hydrogen into the film. The gas sensors could maintain their stability for over 1500 switching cycles. Their high gasochromic performance was attributed to the presence of many voids in the film and the catalytic activity of Pt NPs.

Gasochromic eye-readable H$_2$ sensors are in high demand as they do not require electrical or additional contacts. Furthermore, there is no risk of explosion in high hydrogen gas concentrations [78]. In this regard, amorphous Pd/TiO$_2$/WO$_3$/glass thin films were prepared using a PLD technique. Using a laser (λ = 248 nm) with different incident energies (110, 140, 170, and 200 mJ), thin top layers of anatase TiO$_2$ (a-TiO$_2$) with a high photocatalytic activity were generated and their gasochromic performance was studied at room temperature. Figure 6 shows photographs of different coloring steps over 1 h after exposure to hydrogen gas.
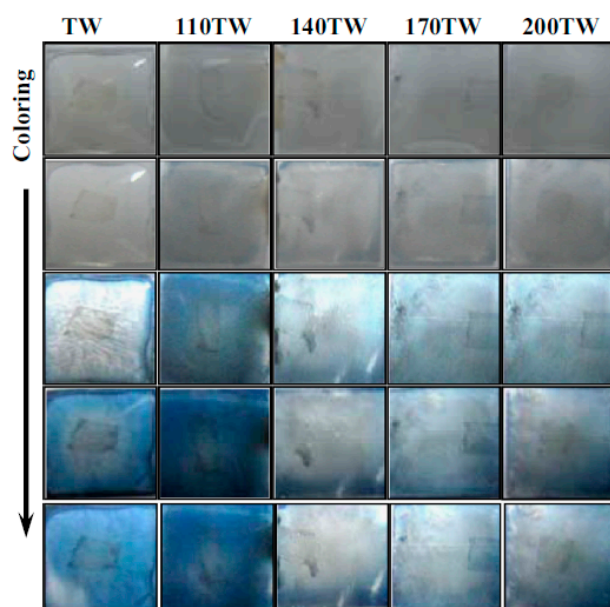

Figure 6. Images of Pd/WO$_3$ sensors during gasochromic coloration (TW is incident energy). (Reprinted with permission from [79]).

Coloring in the sensors started from the edges. The as-synthesized sample (TW) and the 110 TW sample were fully colored after 1 h of exposure to hydrogen gas, however, the former showed a long switching time. This is because the continuous TiO$_2$ layer decreased the interlayer diffusion of hydrogen gas. The poor coloring effect in the samples 140 TW to 200 TW is attributed to their crystalline nature [79].

In another study related to naked-eye gas sensors, rapid gasochromic hydrogen gas sensors were realized using 2D nanoplates of WO$_3$, which were synthesized by a sol-gel method. Subsequently, Pd NPs were deposited by a photochemical deposition method [78]. In a hydrogen atmosphere, the sensors exhibited a visible color change from brown to dark blue—all H$_2$ concentrations could be detected according to an eye-readable gasochromic scheme. Figure 7 shows photographs of 2D WO$_3$-Pd sensors deposited on filter papers and exposed to different concentrations of H$_2$ gas at room temperature. A complete color change occurred at different H$_2$ gas exposure times and concentrations. The 2D WO$_3$/Pd sensors showed fast coloration and bleaching times at all hydrogen concentrations. At 100% H$_2$ concentration, complete color change occurred in 4 s, with 30 s of recovery time. The fast response of the sensor was attributed to the rapid and complete diffusion of H atoms throughout the

WO_3 structure, which caused an increase in the access of W atoms to H atoms in a shorter period of time when compared to 1D materials.
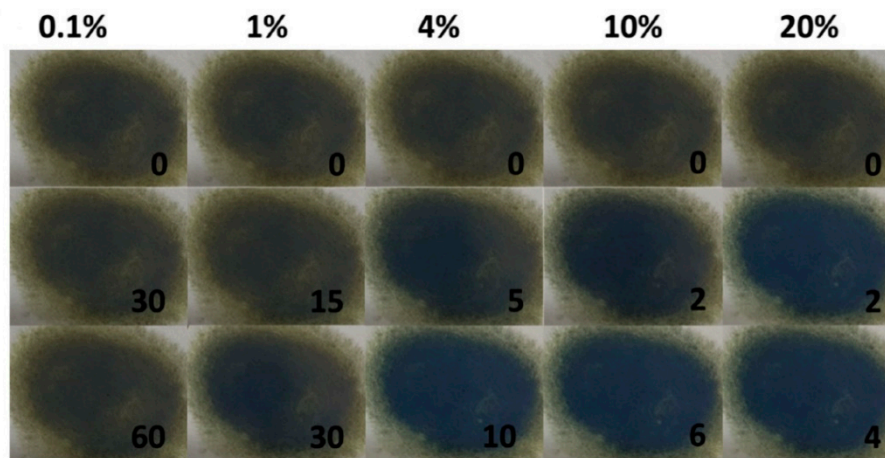
Figure 7. Photographs of 2D WO_3/Pd on filter papers during gasochromic hydrogen gas tests. (Reprinted with permission from [78]).

The limit of detection for the above described gas sensors was 4%, which is considered the lower limit for H_2 explosion in air. Further, the gas sensors exhibited good reproducibility and high stability—their gas sensing mechanism was related to the formation of hydrogen tungsten bronzes (H_xWO_3, x = 0–1) [78].

Yamaguchi and co-workers [80] synthesized Pt/WO_3 thin films using a sol-gel method for eye-readable gasochromic hydrogen sensors. When the sensors were exposed to 1% hydrogen, their transmittance reduced and, in the presence of 100% hydrogen gas, they changed from transparent to blue. The gasochromic phenomenon of these sensors was attributed to the formation of H_xWO_3, which was different in color when compared to WO_3. Hydrogen molecules were split onto hydrogen atoms and, upon subsequent spillover to Pd, tungsten ions were reduced (changing W^{6+} to W^{5+}) and H_xWO_3 was formed. The relevant reactions are as follows [80]:

$$H_2 \xrightarrow{Pt} 2 \tag{4}$$

$$2H \rightarrow 2H^+ + 2e^- \tag{5}$$

$$xH^+ + xe^- + WO_3 \rightarrow H_xWO_3 \tag{6}$$

Kalanur et al. [81] synthesized WO_3-Pd nanocomposites and subsequently deposited them on filters for hydrogen gas sensing at room temperature. Figure 8 shows images of WO_3-Pd nanocomposites when exposed to different concentrations of hydrogen gas. In a H_2 atmosphere, the WO_3-Pd nanocomposite changed its color to blue-gray, which could be easily detected by a naked eye. Color change was strongly dependent on both hydrogen concentration and exposure time. Hydrogen tungsten bronze (H_xWO_3) formation is held to be responsible for color changes in these gas sensors. At 1% and 100% hydrogen concentration, the full coloration times were only 240 s and 45 s, respectively. However, the recovery time was long (~30 min) at all concentrations of hydrogen gas.

Generally, gas sensors with nanowire (NW) morphology exhibit good self-heating effects [82]. In this context, Chen et al. [83] studied the effect of self-heating on the gasochromic response of Pt/WO_3 NW sensors. Changes in the optical properties of Pt-WO_3 NW sensors at λ = 632.8 nm indicated that their coloration response was greatly improved by the self-heating effect, resulting in a high coloration contrast and fast response time (less than 10 ms). The ultrafast gasochromic response time is related to the temperature of WO_3 NWs, which increased to above 200 °C during self-heating cycles. In a hydrogen atmosphere, the absorbed H_2 molecules on the surface of Pt NPs dissociated into H ions and

electrons (Figure 9a). Later, they were transferred to the surfaces of WO_3 NWs by the spillover effect and were subsequently injected into WO_3 NWs. Due to the reaction between injected hydrogen atoms and oxygen atoms in the lattice structure of WO_3, WO_{3-x} xH_2O was formed, which caused coloration in the gas sensor. When the NWs were exposed to oxygen gas or air (Figure 9b), due to the spillover effect of Pt on oxygen gas, the density of free electrons in NWs decreased to a great extent (Figure 9c) which led to instability in the localized water molecules in the body of the WO_3 NW. These localized water molecules decomposed into atomic hydrogen and oxygen species, which subsequently diffused to the NW surface and reacted with foreign oxygen ions to form water vapor, while oxygen species re-filled oxygen vacancies and the sensor regained its initial structure and was bleached [83].
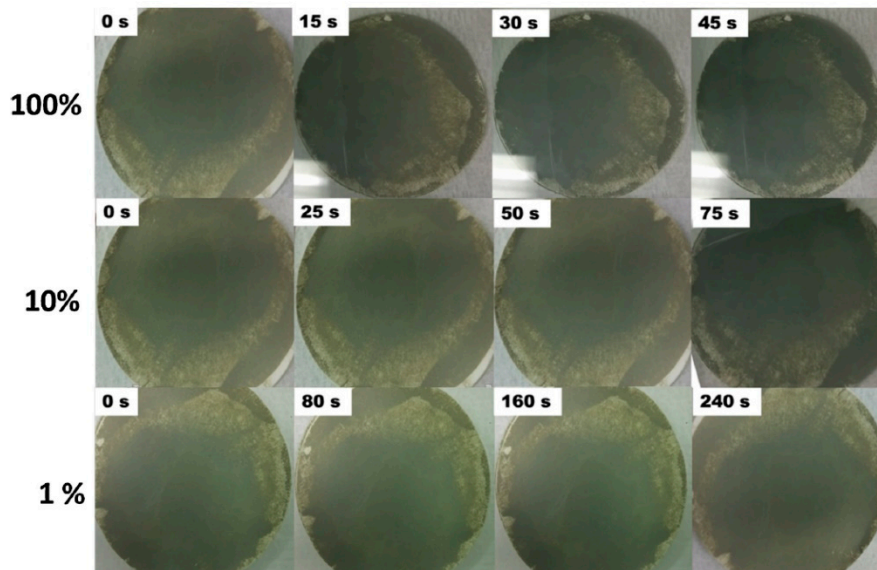
Figure 8. Photographs of WO_3-Pd nanocomposites during gasochromic hydrogen gas tests. (Reprinted with permission from [81]).
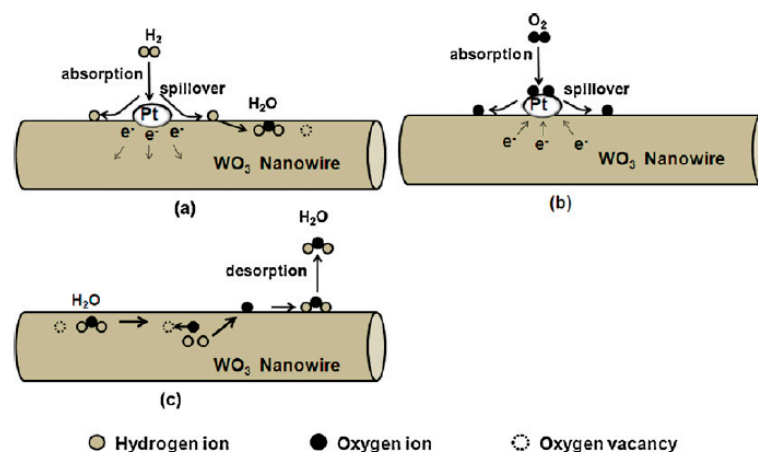

Figure 9. The surface of a Pt/WO_3 nanowire (NW) in (**a**) H_2 gas; (**b**) O_2 gas, and (**c**) during the bleaching process. (Reprinted with permission from [83]).

Optical heating using a laser can also be used to attenuate the gasochromic properties of a sensor. In general, sensor sensitivity decreases, and its response time increases in harsh environments, such as cold areas. In such conditions, heating a gas sensor may increase its performance. In this context, Okazaki et al. [84] reported the hydrogen (4 vol% H_2/N_2 gas) gasochromic performance of sol-gel-prepared Pt/WO_3 films at different temperatures using optical transmittance measurements. They used optical heating with a high-power laser diode to improve the response rate of the films

at low temperatures. Sensitivity was defined as the percentage of change in the transmitted light in the presence of the target gas. More than 60% change was observed in the transmittance at room temperature with a response time of ~10 s. The sensor exhibited lower sensitivity at lower temperatures, even though an acceptable sensitivity (>40%) was still obtained at −40 °C. During the optical heating of sensors with laser diodes, reaction kinetics are enhanced, resulting in their good sensitivity.

In another study on NWs, Luo et al. [85] studied the gasochromic phenomenon in Pt/WO_3 NWs. When H_2 gas was injected, it dissociated on Pt into hydrogen species and subsequently reacted with absorbed oxygen ions to form H_2O molecules. The hydrogen species could also react with the oxygen atoms of WO_3 to form localized water molecules. Therefore, coloration could be attributed to the formation of a new structure, namely $WO_{3-x} \cdot xH_2O$, which indicates the coexistence of localized water molecules and oxygen vacancies. Furthermore, coloration was related to photon absorption involving both the defect band in the bandgap and the two tails of the valence and conduction bands of the sensing layer.

Noble metals not only increase gas sensitivity but also significantly reduce the response and recovery times [30] of gas sensors. However, surface poisoning of noble metals can decrease the coloring performance of WO_3 gasochromic sensors. Poisoning may be ascribed to the adsorption of some gases, such sulfur and CO, leading to a reduction in the number of sites available for hydrogen dissociation and therefore a poor gasochromic performance. Luo et al. [86] reported a decrease in the gasochromic coloration of Pt-coated WO_3 NW films due to the poisoning of Pt NPs when held in air for long time periods. $W_{18}O_{49}$ NW films were prepared by thermal evaporation. The samples were then annealed in air at 600 °C for 5 h to obtain WO_3 NW films. Finally, Pt NPs were sputter-deposited onto the surfaces of WO_3 NWs. When Pt/WO_3 NWs were exposed to air for a long time, the Pt and WO_3 surfaces were covered by oxygen atoms, resulting in a drastic decrease in the number of surface sites available for the adsorption and dissociation of H_2 molecules. Accordingly, the response and response times decreased. The poisoned Pt catalyst led to a degraded response, which resulted in a concomitant increase in the response time. To restore the gasochromic properties of the NWs, the samples were subjected to annealing. After annealing, the samples exhibited an increasingly deep blue color (Figure 10a–c). The change in transmittance (ΔT) at $\lambda = 632.8$ nm increased from about 50% to more than 70% after annealing (Figure 10d). Therefore, maintaining a high vacuum space or oxygen-free atmosphere with Ar and N_2 gases is suggested for prolonging the lifetime of gas sensors.
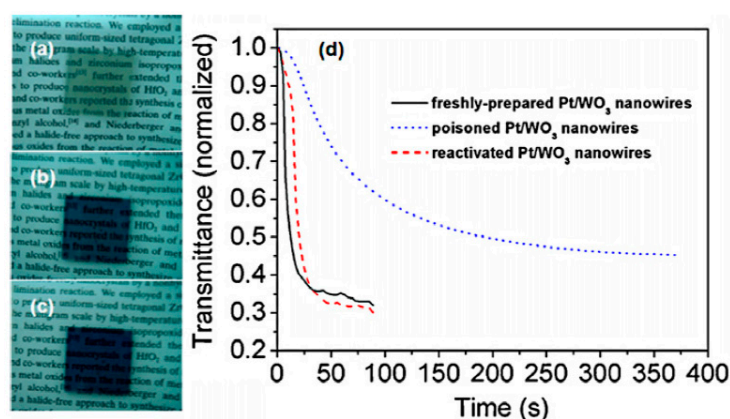

Figure 10. (**a**) The bleached state; (**b**) colored state before poisoning, and (**c**) colored state after annealing of Pt/WO_3 NW sensors; (**d**) Light transmittance spectra of Pt/WO_3 NW sensors. (Reprinted with permission from [86]).

Not only NWs but also nanofibers (NFs) can be used for gasochromic studies. Tavakoli et al. [87] reported the gasochromic properties of $PdCl_2$-decorated WO_3 nanofibers fabricated by electrospinning. Figure 11 reveals the changes in the color of NFs with time in the presence of different concentrations of hydrogen gas. The initial pale yellow color of the sensor changed to blue, and hydrogen was detected

in ~60–90 s. With longer exposure times, the color intensified to some extent and the blue parts covered most of the surfaces. When hydrogen reaches the $PdCl_2$ solution, due to interaction between hydrogen and $PdCl_2$, Pd ions gradually begin to reduce to Pd. Then, in a spillover process, H_2 dissociated into two H^+ atoms and two free electrons, which diffused into the WO_3 lattice and occupied the available sites. As a result, tungsten oxide bronze ($H_xW^{6+}_{1-x}W^{5+}_xO_3$), which is a mixture of W^{6+} and W^{5+}, was formed. W^{5+} is blue in color, while WO_3 (W^{6+}) is pale yellow in color (Figure 12).
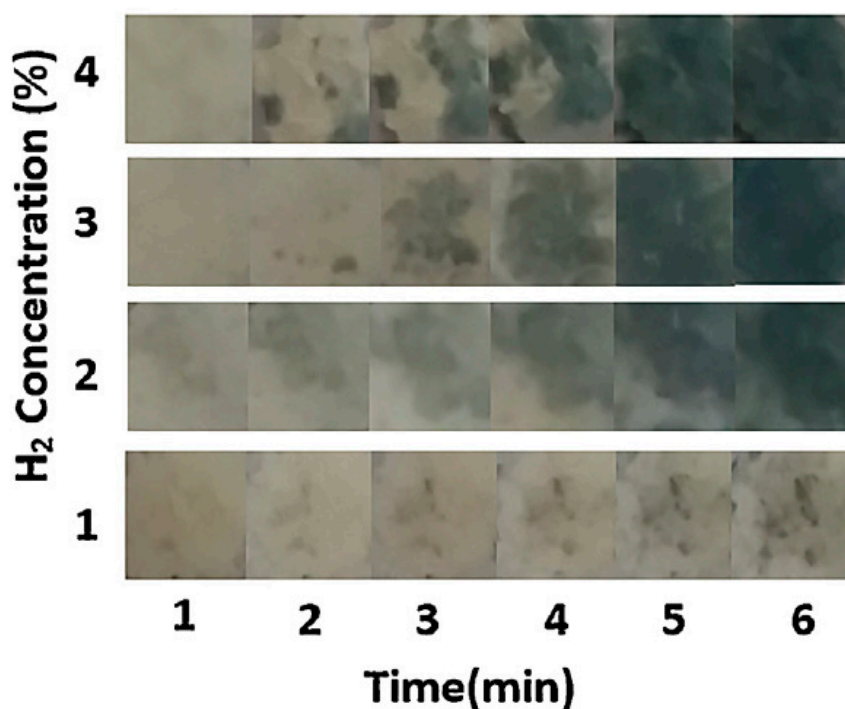
Figure 11. Color changes in WO_3 nanofibers (NFs) when exposed to 1%, 2%, 3%, and 4% hydrogen. (Reprinted with permission from [87]).
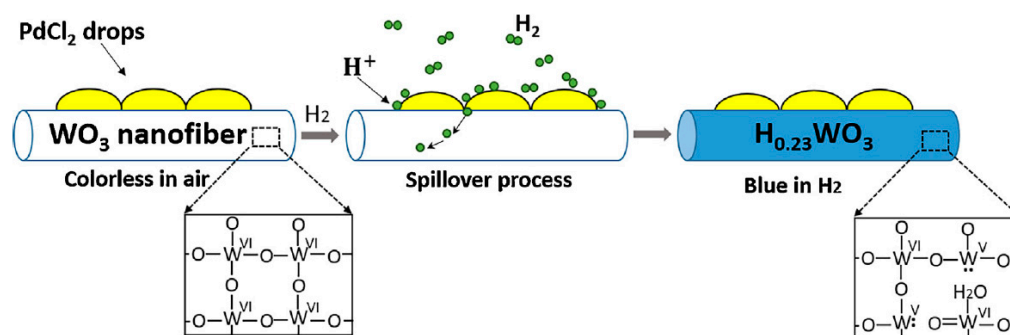

Figure 12. Illustration of the gasochromic mechanism of $PdCl_2$-decorated WO_3 nanofibers. (Reprinted with permission from [87]).

Gas sensors with nanorod (NR) morphology have been used for the gasochromic detection of hydrogen gas. Wisitsoorat et al. [88] used Pd/WO_3 NRs prepared by RF magnetron sputtering for the gasochromic sensing of hydrogen gas. The optical absorbance of the gas sensors was continuously monitored over a wavelength range of 650 to 1000 nm. Upon H_2 exposure at 150 °C, the absorbance of the WO_3 NRs increased over the entire visible-NIR region. Changes in absorbance correspond to the gasochromic phenomenon, in which transparent W^{6+} cations in WO_3 were reduced to W^{5+} by the electrons generated during the catalyzed hydrogen reduction reaction.

Most gasochromic WO_3 sensors show slow coloring/bleaching times, which is a limitation for their practical application. Chan et al. [89] prepared nanostructured WO_3 films by a sol-gel method

and spin coating. Pt was then sputtered onto the WO_3 films. The transmission of the produced films at λ = 550 nm was measured when they were exposed to hydrogen and air. The gas sensors exhibited excellent gasochromic performance with good coloration changes and fast response dynamics at room temperature. The response times of the coloring/bleaching processes of the Pt/WO_3 film were very fast and less than 5 s. The rapid dynamics of the gas sensors are related to their structural features and morphology. In a separate study, Hsu et al. [90] fabricated Pt/WO_3 thin films by PLD and sputtering methods. Their gasochromic performance at room temperature was determined from optical transmittance measurements at λ = 550 nm at different H_2 gas concentrations. Upon injecting H_2 gas, the color of the film changed to dark blue very fast. In fact, the film response time to 5% H_2 was less than 1 s, which clearly demonstrates its very fast dynamics.

Chen et al. [91] designed a novel $Pd-WO_3$/graphene/Si gasochromic sensor with a tandem structure for detecting hydrogen at room temperature. A laser (λ = 980 nm) was used as the light source to study the transmittance of the sensor in the presence of hydrogen and air. Based on changes in its transmittance, the gas sensor was able to detect hydrogen gas at concentrations as low as 0.05 vol%, with response time and recovery time less than 13 s and 43 s, respectively. Figure 13a shows photographs of the $Pd-WO_3$ gas sensor on glass substrates in the bleached state and after exposure to 4 vol% H_2/Ar gas. Figure 13b shows the transmittance spectra of the sensor film in the bleached and colored states. The difference in transmittance between the bleached and colored states increased with an increase in the wavelength. The maximum reduction of 72% ($\Delta T/T_0$ = 72%) was observed at a wavelength of ~1000 nm.
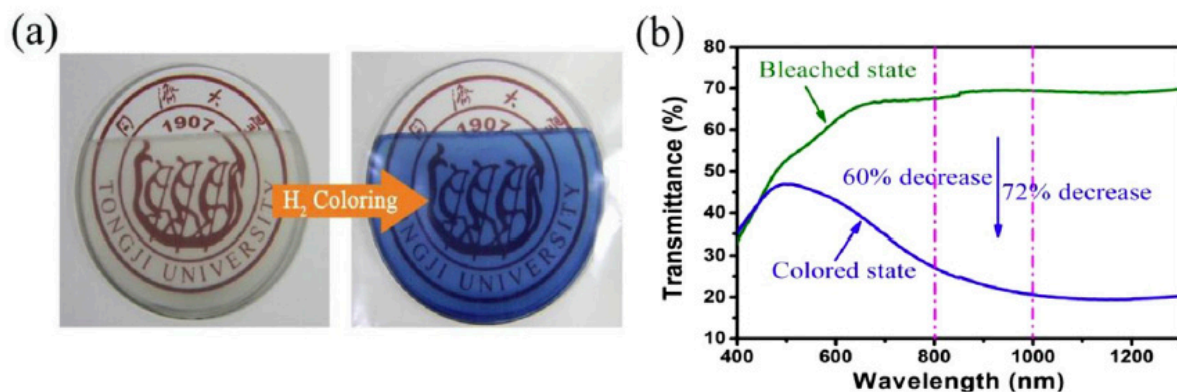

Figure 13. (**a**) Photographs of the $Pd-WO_3$/graphene/Si sensor before and after exposure to 4 vol% H_2/Ar gas; (**b**) Transmittance spectra of the $Pd-WO_3$/graphene/Si sensor in the bleached and colored states. (Reprinted with permission from [91]).

In hydrogen atmosphere, one hydrogen molecule can be dissociated into H atoms (on Pd) and hydrogen atoms react with WO_3, producing H_xWO_3 (x ~ 0–1). Thus, the color of the film changed to dark blue. The relevant reaction can be written as follows [92]:

$$WO_3 + xH_2 \rightarrow WO_{3-x}.xH_2O \qquad (7)$$

The reaction of the bleaching process is as follows:

$$WO_{3-x}. xH_2O + x_2O_2 \rightarrow WO_3 + xH_2O \qquad (8)$$
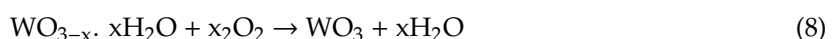
Sensors with reversible behavior, good selectivity to hydrogen gas, and a low working temperature can potentially be used to detect hydrogen gas in practical scenarios.

The effect of water vapor on the gasochromic phenomenon has also been investigated. E-beam evaporated WO_3 films covered by Pt on glass substrates were used for gasochromic studies. In a humid atmosphere, the films contained large amounts of water, and the coloration response rate was strongly dependent on the relative humidity of the atmosphere. This was due to site blocking by H_2O

vapor. Therefore, a decrease in the coloration rate was observed with an increase in the H_2O vapor pressure [93].

Ranjbar et al. [94] fabricated WO_3 films by PLD, and Pd NPs were coated on WO_3 using an electrodeless method. The effect of Pd growth time (1–40 min) on the response and recovery times of the gas sensors was studied. Optical changes in the presence of H_2 gas were so complex when two different mechanisms, including bleaching due to the formation of PdH_x and the coloring of WO_3 itself, occur together. As a result, with the injection of 10% H_2/Ar gas, the optical density of the samples decreased rapidly and then gradually increased during the process of coloration, which was attributed to the rapid formation of the PdH_x complex by hydrogen absorption on Pd NPs. The shortest coloring/bleaching rates were observed with the sample prepared at a growth time of 2 min. At shorter growth times, the number of Pd NPs formed was too little to indicate good catalytic activity. Meanwhile, in the sample prepared over longer growth times, large-sized Pd particles were formed. They exhibited a limited catalytic activity as compared to those of small Pd NPs, resulting in longer reaction dynamics—accordingly, only for a critical growth time of 2 min, as-grown Pd particles had enough sizes and concentrations. Gasochromic studies demonstrated that that the samples deposited in an oxygen environment exhibited good coloring response, which was due to the amorphous structure and near stoichiometric nature of these samples.

Yamamoto et al. [95] investigated the effect of composition and structure of WO_3 sensing films on the gasochromic coloration of sputter deposited WO_3 films with various O/W atomic ratios from 1.5 to 3.0. In a hydrogen atmosphere, stoichiometric WO_3 films with an amorphous structure showed enhanced gasochromic coloration when compared to those of non-stoichiometric WO_3 films with an amorphous structure or with a crystalline structure. Therefore, it was concluded that gasochromic coloration strongly depends on the composition and structure of WO_3 films. In another study on the composition of gasochromic sensors, Pt-coated $(WO_3)_{1-x}$ $(Nb_2O_5)_x$ thin films were prepared by PLD [96] and their gasochromic coloration properties were studied using an UV-Vis spectrophotometer at room temperature in H_2/N_2 gas mixtures containing 1–100 mol % H_2. Because Nb itself exists in various oxidation states from +5 to +1, it is expected that Nb_2O_5 improves tungsten oxidation and thus enhances the gasochromic characteristics of WO_3. The results showed that the $(WO_3)_{0.85}(Nb_2O_5)_{0.15}$/Pt gas sensor exhibited the shortest response time (30 s)—this gas sensor exhibited the highest transmittance change (ΔT) of 30%. Ranjbar et al. [97] prepared $(WO_3)_{1-x}$ $(V_2O_5)_x$ (x = 0, 0.09, 0.17, 0.23, 0.29, and 0.33) mixed powders by PLD. It was reported that the ratio of W^{5+}/W^{6+} increased upon increasing the amount of vanadium in the produced films. The sample with x = 0.09 showed both deeper and faster color changes. The weak responses of samples with x > 0.09 are related to the low amount of W^{5+} in the films and also to the low porosity of the films. W^{5+} ions are generated due to the interaction between hydrogen ions and electrons with the initial W^{6+} ions. Therefore, a primarily high concentration of W^{6+} is important for switching on the gasochromic response upon hydrogen exposure [97].

The sensor preparation method also affects the performance of gas sensors. Ranjbar et al. [98] prepared two types of WO_3 films by PLD and sol-gel methods. Subsequently, using $PdCl_2$, Pd-decorated WO_3 nanostructures were prepared. Gasochromic investigations showed that the level of coloring depends on the amount of $PdCl_2$ as well as the synthesis method. Sol-gel-prepared Pd-decorated WO_3 showed weak gasochromic properties. In fact, it exhibited a compact and dense structure, owing to which Pd ions hardly diffuse into the WO_3 layer and remain on the surface. Furthermore, the diffusion of hydrogen atoms is greatly limited at the top of Pd-decorated WO_3 sol-gel samples. In contrast, Pd-decorated WO_3 gas sensors prepared by PLD exhibited a highly porous nature with a columnar open structure, which improved the penetration of the $PdCl_2$ solution into their pores, leading to the growth of Pd NPs over pore walls. Furthermore, such sensors exhibited a large surface area and provided more adsorption sites for hydrogen gas, resulting in better gasochromic characteristics [98].

In an interesting study, Garavand et al. [99] investigated the gasochromic properties of colloidal WO_3 NPs synthesized by a PLD technique in deionized water using a laser (λ = 1064 nm) at different pulse energies of E_1 = 160, E_2 = 370 and E_3 = 500 mJ/pulse. A $PdCl_2$ solution was added to colloidal

tungsten oxide NPs, after which a laser was used to reduce Pd^{2+} to metallic Pd. The reduction of Pd NPs to Pd^{2+} did not occur effectively at E_1, while at E_3, all Pd^{2+} ions were effectively reduced to metallic Pd. As more unreduced Pd^{2+} ions are available in the sample prepared at E_1, it exhibited greater irreversibility as compared to those of samples prepared at higher laser pulse energies. Gasochromic coloration in the sensors was attributed to the formation of W^{5+} ions in the presence of hydrogen gas. Optical absorption by W^{5+} ions resulted in the colloidal solution changing from a bleached state to a blue-colored state. The optical properties of W^{5+} centers are dependent on oxygen-tungsten bonds. The absorption peaks at 977 and 630 nm were attributed to different oxygen-tungsten bonds that led to the formation of different energy levels for W^{5+} centers.

Gasochromic sensors with Au decoration are rarely reported for hydrogen gas detection. Ahmad et al. [30] used nanostructured Au/WO_3 thin films for the gasochromic detection of hydrogen gas. At 200 °C, it was observed that adsorption increased by ~2.5% in the presence of 0.06% H_2. The response times to 0.06% and 1% H_2 were 180 s and 120 s, respectively, and the recovery time was ~5 min at both concentrations. The gasochromic reaction occurred due to the reduction of W^{6+} ions (transparent) to W^{5+} ions (blue). Repeated gasochromic cycles and long-term storage led to structural collapse and catalyst (Au) poisoning, resulting in an increase in the response and recovery times and also partial gasochromic irreversibility.

Sometimes, sensor surfaces can also affect their gasochromic properties. Li et al. [100] synthesized Pt/WO_3 nanosphere films by a sol-gel method. The color of the nanospheres changed rapidly in 5 to 10 s from light yellow to blue in the presence of hydrogen. Upon removal of hydrogen gas, the films were bleached quickly (10 to 20 s). In the second cycle, the response time was ~40 s. The WO_3 nanosphere films maintained their crystal structure after hydrogen gasochromic testing. The high response of the film was attributed to the high surface area of WO_3 nanospheres, which favors coloration. Further, it was reported that the WO_3/Pt films were inert to other gases such as NH_3, alcohols, and acetone at room temperature, which demonstrates their good selectivity.

Composite films with nanoporous structures can exhibit good gasochromic performance. Li et al. [101] prepared with Pd-loaded nanoporous WO_3/SiO_2 composite films by sol-gel dip coating. Their coloring (R_c) and bleaching (R_b) rates were calculated as linear slopes of transmittance (T) as functions of time (t) as follows [101]:
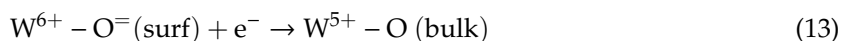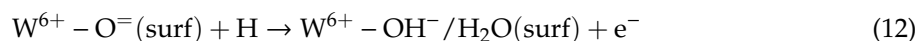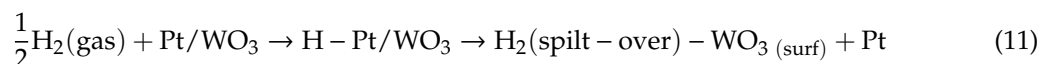
$$R_c(\%/s) = \frac{(T_c - T_{c0})}{t_c - t_{c0}} \times 100 \tag{9}$$

$$R_b(\%/s) = \frac{(T_b - T_{b0})}{t_b - t_{b0}} \times 100 \tag{10}$$

The subscripts "c" and "b" refer to colored and bleached states, respectively. The coloring rate of WO_3 films was very fast. The bleaching rate of Pd/WO_3-SiO_2 (44.1%/s) was significantly higher than that of pristine WO_3 films (7.18%/s), demonstrating remarkably faster reaction kinetics in the former sensor. The coloring rate of Pd/WO_3-SiO_2 films was 14.8%/s, while that of pristine WO_3 was only ~2.84%/s. Furthermore, the Pd/WO_3-SiO_2 sensor showed good reversibility. The gasochromic characteristics of these sensors are related to the diffusion of H atoms, which are strongly dependent on the microstructure of WO_3 films and presence of the Pd catalyst. Upon adding SiO_2 to a WO_3 matrix, a nanoporous structure with a high surface to volume ratio was obtained, which greatly enhanced the diffusion of hydrogen atoms. In fact, in the nanoporous structure, WO_3 particles were loaded with Pd catalyst around the SiO_2 network, where SiO_2 acted as a supporting framework to form a nanoporous and stable composite structure.

In another study on porous structures, WO_3 thin films were coated with Pt by reactive sputtering, and Pt NPs were coated on WO_3 by spin coating [102]. Pt/WO_3 layers with a porous nature showed high transmittance. Upon exposure to hydrogen, a deep blue coloration was observed. A similar study was conducted by Chan et al. [67]. The gasochromic coloration mechanism of these sensors is related to the reduction of W^{6+} (transparent) centers in the WO_3 crystal lattice to W^{5+} (blue color) and the

formation of blue tungsten bronze ($H_x WO_3$) in the presence of hydrogen gas. The relevant reactions for the reduction of W^{6+} to W^{5+} can be illustrated as follows:

$$\frac{1}{2} H_2(\text{gas}) + Pt/WO_3 \rightarrow H - Pt/WO_3 \rightarrow H_2(\text{spilt} - \text{over}) - WO_{3 \ (\text{surf})} + Pt \tag{11}$$

$$W^{6+} - O^=(\text{surf}) + H \rightarrow W^{6+} - OH^-/H_2O(\text{surf}) + e^- \tag{12}$$

$$W^{6+} - O^=(\text{surf}) + e^- \rightarrow W^{5+} - O \ (\text{bulk}) \tag{13}$$

4. Conclusions and Outlook

In this review, we discussed nanostructured gasochromic WO_3 for the detection of hydrogen gas. The effects of substrate, crystallinity, preparation method, and morphology on the sensing properties of these sensors were discussed and explained. Gasochromic WO_3 gas sensors need noble metals such as Pd, Pt, and Au for the catalytic dissociation of hydrogen molecules and rapid fast detection of hydrogen gas. Most gasochromic sensors work at low or room temperatures and, therefore, significantly decrease the risk of explosion of hydrogen gas. Furthermore, they can be fabricated on flexible substrates and, hence, can be used for detecting the leakage of hydrogen gas from pipelines. However, gasochromic sensors generally exhibit a poor performance at low H_2 concentrations, under which conditions the color change is very slow or cannot be detected by a naked eye. Therefore, for very low concentrations of hydrogen gas, resistivity-based gas sensors may be a better choice. For practical applications of gasochromic sensors, color changes in gasochromic WO_3 gas sensors should be visible to the naked eye. To achieve this objective, high-performance gasochromic sensors with a high surface area, engineered design, and appropriate amount of noble metals should be synthesized using novel protocols. Such gas sensors not only exhibit color changes in the visible light range, but also show fast dynamics, which are vital for the detection of hydrogen, an explosive gas.

References

1. Noh, H.-J.; Kim, H.-J.; Park, Y.M.; Park, J.-S.; Lee, H.-N. Complex behavior of hydrogen sensor using nanoporous palladium film prepared by evaporation. *Appl. Surf. Sci.* **2019**, *480*, 52–56. [CrossRef]
2. Kumar, A.; Kumar, A.; Chandra, R. Fabrication of porous silicon filled Pd/SiC nanocauliflower thin films for high performance H_2 gas sensor. *Sens. Actuators B Chem.* **2018**, *264*, 10–19. [CrossRef]
3. Wu, C.-H.; Zhu, Z.; Huang, S.-Y.; Wu, R.-J. Preparation of palladium-doped mesoporous WO_3 for hydrogen gas sensors. *J. Alloys Compd.* **2019**, *776*, 965–973. [CrossRef]
4. Boon-Brett, L.; Bousek, J.; Castello, P.; Salyk, O.; Harskamp, F.; Aldea, L.; Tinaut, F. Reliability of commercially available hydrogen sensors for detection of hydrogen at critical concentrations: Part I-Testing facility and methodologies. *Int. J. Hydrogen Energy* **2008**, *33*, 7648–7657. [CrossRef]
5. Sanger, A.; Kumar, A.; Kumar, A.; Chandra, R. Highly sensitive and selective hydrogen gas sensor using sputtered grown Pd decorated MnO_2 nanowalls. *Sens. Actuators B Chem.* **2016**, *234*, 8–14. [CrossRef]
6. Xu, B.; Li, P.; Wang, D.; Zhao, C.-L.; Dai, J.; Yang, M. Hydrogen sensor based on polymer-filled hollow core fiber with Pt-loaded WO_3/SiO_2 coating. *Sens. Actuator B Chem.* **2017**, *245*, 516–523. [CrossRef]
7. Harley-Trochimczyk, A.; Chang, J.; Zhou, Q.; Dong, J.; Pham, T.; Worsley, M.A.; Maboudian, R.; Zettl, A.; Mickelson, W. Catalytic hydrogen sensing using microheated platinum nanoparticle-loaded graphene aerogel. *Sens. Actuator B Chem.* **2015**, *206*, 399–406. [CrossRef]

8. Li, Y.; Li, X.; Tang, Z.; Tang, Z.; Yu, J.; Wang, J. Hydrogen sensing of the mixed-potential-type MnWO4/YSZ/Pt sensor. *Sens. Actuator B Chem.* **2015**, *206*, 176–180. [CrossRef]

9. Sil, D.; Hines, J.; Udeoyo, U.; Borguet, E.J. Palladium nanoparticle-based surface acoustic wave hydrogen sensor. *ACS Appl. Mater. Interfaces* **2015**, *7*, 5709–5714. [CrossRef] [PubMed]

10. Mirzaei, A.; Sun, G.-J.; Lee, J.K.; Lee, C.; Choi, S.; Kim, H.W. Hydrogen sensing properties and mechanism of NiO-Nb2O5 composite nanoparticle-based electrical gas sensors. *Ceram. Int.* **2017**, *43*, 5247–5254. [CrossRef]

11. Kim, S.; Song, Y.; Lee, Y.-I.; Cho, Y.-H. Thermochemical hydrogen sensor based on Pt-coated nanofiber catalyst deposited on pyramidally textured thermoelectric film. *Appl. Surf. Sci.* **2017**, *415*, 119–125. [CrossRef]

12. Hübert, T.; Boon-Brett, L.; Black, G.; Banach, U. Hydrogen sensors-A review. *Sens. Actuators B Chem.* **2011**, *157*, 329–352. [CrossRef]

13. Ishihara, R.; Yamaguchi, Y.; Tanabe, K.; Makino, Y.; Nishio, K. Preparation of Pt/WO$_3$-coated polydimethylsiloxane membrane for transparent/flexible hydrogen gas sensors. *Mater. Chem. Phys.* **2019**, *226*, 226–229. [CrossRef]

14. Kabcum, S.; Channei, D.; Tuantranont, A.; Wisitsoraat, A.; Liewhiran, C.; Phanichphant, S. Ultra-responsive hydrogen gas sensors based on PdO nanoparticle-decorated WO$_3$ nanorods synthesized by precipitation and impregnation methods. *Sens. Actuators B Chem.* **2016**, *226*, 76–89. [CrossRef]

15. Mirzaei, A.; Leonardi, S.G.; Neri, G. Detection of hazardous volatile organic compounds (VOCs) by metal oxide nanostructures-based gas sensors: A review. *Ceram. Int.* **2016**, *42*, 15119–15141. [CrossRef]

16. Mirzaei, A.; Neri, G. Microwave-assisted synthesis of metal oxide nanostructures for gas sensing application: A review. *Sens. Actuators B Chem.* **2016**, *237*, 749–775. [CrossRef]

17. Mirzaei, A.; Hashemi, B.; Janghorban, K. α-Fe2O3 based nanomaterials as gas sensors. *J. Mater. Sci. Mater. Electron.* **2016**, *27*, 3109–3144. [CrossRef]

18. Maciak, E.; Pustelny, T. An optical ammonia (NH3) gas sensing by means of Pd/CuPc interferometric nanostructures based on white light interferometry. *Sens. Actuators B Chem.* **2013**, *189*, 230–239. [CrossRef]

19. Hu, J.; Wang, L.; Zhang, P.; Liang, C.; Shao, G. Construction of solid-state Z-scheme carbon-modified TiO$_2$/WO$_3$ nanofibers with enhanced photocatalytic hydrogen production. *J. Power Source* **2016**, *328*, 28–36. [CrossRef]

20. Li, Z.; Yang, M.; Dai, J.; Wang, G.; Huang, C.; Tang, J.; Hu, W.; Song, H.; Huang, P. Optical fiber hydrogen sensor based on evaporated Pt/WO$_3$ film. *Sens. Actuators B Chem.* **2015**, *206*, 564–569. [CrossRef]

21. Huang, B.-R.; Lin, T.-C.; Liu, Y.-M. WO$_3$/TiO$_2$ core-shell nanostructure for high performance energy-saving smart windows. *Solar Energy Mater. Solar Cells* **2015**, *133*, 32–38. [CrossRef]

22. Tahir, M.B.; Sagir, M.; Shahzad, K. Removal of acetylsalicylate and methyl-theobromine from aqueous environment using nano-photocatalyst WO$_3$-TiO$_2$ @g-C3N4 composite. *J. Hazard. Mater.* **2019**, *363*, 205–213. [CrossRef] [PubMed]

23. Wang, Y.; He, B.; Wang, H.; Xu, J.; Ta, T.; Li, W.; Wang, Q.; Yang, S.; Tang, Y.; Zou, B. Transparent WO$_3$/Ag/WO$_3$ electrode for flexible organic solar cells. *Mater. Lett.* **2017**, *188*, 107–110. [CrossRef]

24. Faia, P.M.; Libardi, J. Response to humidity of TiO$_2$:WO$_3$ sensors doped with V$_2$O$_5$: Influence of fabrication route. *Sens. Actuators B Chem.* **2016**, *236*, 682–700. [CrossRef]

25. Sun, J.; Sun, L.; Han, N.; Pan, J.; Liu, W.; Bai, S.; Feng, Y.; Luo, R.; Li, D.; Chen, A. Ordered mesoporous WO$_3$/ZnO nanocomposites with isotype heterojunctions for sensitive detection of NO$_2$. *Sens. Actuators B Chem.* **2019**, *285*, 68–75. [CrossRef]

26. Hočevar, M.; Krašovec, U.O. Cubic WO$_3$ stabilized by inclusion of Ti: Applicable in photochromic glazing. *Solar Energy Mater. Solar Cells* **2016**, *154*, 57–64. [CrossRef]

27. Ataalla, M.; Afify, A.S.; Hassan, M.; Abdallah, M.; Milanova, M.; Aboul-Enein, H.Y.; Mohamed, A. Tungsten-based glasses for photochromic, electrochromic, gas sensors, and related applications: A review. *J. Non-Cryst. Solids* **2018**, *491*, 43–54. [CrossRef]

28. Bange, K. Colouration of tungsten oxide films: A model for optically active coatings. *Sol. Energy Mater. Sol. Cells* **1999**, *58*, 1–131. [CrossRef]

29. Vogt, T.; Woodward, P.M.; Hunter, B.A. The high-temperature phases of WO$_3$. *J. Solid State Chem.* **1999**, *144*, 209–215. [CrossRef]

30. Ahmad, M.Z.; Sadek, A.Z.; Yaacob, M.; Anderson, D.P.; Matthews, G.; Golovko, V.B.; Wlodarski, W. Optical characterisation of nanostructured Au/WO$_3$ thin films for sensing hydrogen at low concentrations. *Sens. Actuators B Chem.* **2013**, *179*, 125–130. [CrossRef]

31. Pandurang, A. *Transition Metal Oxide Thin Film Based Chromogenics and Devices*, 1st ed.; Elsevier: Amsterdam, The Netherlands, 2017.

32. Opara Krašovec, U.; Šurca Vuk, A.; Orel, B. IR Spectroscopic studies of charged-discharged crystalline WO_3 films. *Electrochim. Acta* **2001**, *46*, 1921–1929. [CrossRef]

33. Inouye, A.; Yamamoto, S.; Nagata, S.; Yoshikawa, M.; Shikama, T. Hydrogen behavior in gasochromic tungsten oxide films investigated by elastic recoil detection analysis. *Nucl. Instrum. Methods. Phys. Res. B* **2008**, *266*, 301–307. [CrossRef]

34. Gogova, D.; Thomas, L.-K.; Camin, B. Comparative study of gasochromic and electrochromic effect in thermally evaporated tungsten oxide thin films. *Thin Solid Films* **2009**, *517*, 3326–3331. [CrossRef]

35. Domaradzki, J.; Kaczmarek, D.; Wojcieszak, D.; Mazur, M. Investigations of reversible optical transmission in gasochromic (Ti-V-Ta) Ox thin film for gas sensing applications. *Sens. Actuators B Chem.* **2014**, *201*, 420–425. [CrossRef]

36. Liu, B.; Cai, D.; Liu, Y.; Wang, D.; Wang, L.; Wang, Y.; Li, H.; Li, Q.; Wang, T. Improved room-temperature hydrogen sensing performance of directly formed Pd/WO_3 nanocomposite. *Sens. Actuators B Chem.* **2014**, *193*, 28–34. [CrossRef]

37. Sanger, A.; Kumar, A.; Kumar, A.; Jaiswal, J.; Chandra, R. A fast response/recovery of hydrophobic Pd/V_2O_5 thin films for hydrogen gas sensing. *Sens. Actuators B Chem.* **2016**, *236*, 16–26. [CrossRef]

38. Rizzo, G.; Arena, A.; Bonavita, A.; Donato, N.; Neri, G.; Saitta, G. Gasochromic response of nanocrystalline vanadium pentoxide films deposited from ethanol dispersions. *Thin Solid Films* **2010**, *518*, 7124–7127. [CrossRef]

39. Ho, Y.; Chang, C.; Wei, D.; Dong, C.; Chen, C.; Chen, J.; Jang, W.; Hsu, C.; Chan, T.; Kumar, K. Characterization of gasochromic vanadium oxides films by X-ray absorption spectroscopy. *Thin Solid Films* **2013**, *544*, 461–465. [CrossRef]

40. Shanak, H.; Schmitt, H.; Nowoczin, J.; Ehses, K.-H. Effect of O_2 partial pressure and thickness on the gasochromic properties of sputtered V_2O_5 films. *J. Mater. Sci.* **2005**, *40*, 3467–3474. [CrossRef]

41. Jang, W.-L.; Lu, Y.-M.; Lu, Y.-R.; Chen, C.-L.; Dong, C.-L.; Chou, W.-C.; Chen, J.-L.; Chan, T.-S.; Lee, J.-F.; Pao, C.-W. Effects of oxygen partial pressure on structural and gasochromic properties of sputtered VOx thin films. *Thin Solid Films* **2013**, *544*, 448–451. [CrossRef]

42. Hosseini, M.; Ranjbar, M. Plasmonic $Au-MoO_3$ colloidal nanoparticles by reduction of $HAuCl_4$ by blue MoOx nanosheets and observation of the gasochromic property. *Plasmonics* **2018**, *13*, 1897–1906. [CrossRef]

43. Kalanur, S.S.; Yoo, I.-H.; Seo, H. Pd on MoO3 nanoplates as small-polaron-resonant eye-readable gasochromic and electrical hydrogen sensor. *Sens. Actuators B Chem.* **2017**, *247*, 357–365. [CrossRef]

44. Chang, C.-C.; Luo, J.-Y.; Chen, T.-K.; Yeh, K.-W.; Huang, T.-W.; Hsu, C.-H.; Chao, W.-H.; Ke, C.-T.; Hsu, P.-C.; Wang, M.-J. Pulsed laser deposition of (MoO3)1-x (V_2O_5)x thin films: Preparation, characterization and gasochromic studies. *Thin Solid Films* **2010**, *519*, 1552–1557. [CrossRef]

45. Imani, M.; Tadjarodi, A. H_2S gasochromic effect of mixed ammonium salts of phosphomolybdate nanoparticles synthesized by microwave assisted technique. *Sens. Actuators B Chem.* **2016**, *237*, 715–723. [CrossRef]

46. Fomanyuk, S.; Kolbasov, G.Y.; Chernii, V.Y.; Tretyakova, I. Gasochromic α, β–Ni (OH)2 films for the determination of CO and chlorine content. *Sens. Actuators B Chem.* **2017**, *244*, 717–726. [CrossRef]

47. Orel, B.; Grošelj, N.; Krašovec, U.O.; Gabršček, M.; Bukovec, P.; Reisfeld, R. Gasochromic effect of palladium doped peroxopolytungstic acid films prepared by the sol-gel route. *Sens. Actuators B Chem.* **1998**, *50*, 234–245. [CrossRef]

48. Orel, B.; Krašovec, U.O.; Grošelj, N.; Kosec, M.; Dražič, G.; Reisfeld, R. Gasochromic behavior of sol-gel derived Pd doped peroxopolytungstic acid (W-PTA) nano-composite films. *J. Sol-Gel Sci. Technol.* **1999**, *14*, 291–308. [CrossRef]

49. Ngene, P.; Radeva, T.; Slaman, M.; Westerwaal, R.J.; Schreuders, H.; Dam, B. Seeing hydrogen in colors: Low-cost and highly sensitive eye readable hydrogen detectors. *Adv. Funct. Mater.* **2014**, *24*, 2374–2382. [CrossRef]

50. Seo, C.; Cheong, H.; Lee, S.-H. Color change of V_2O_5 thin films upon exposure to organic vapors. *Sol. Energy Mater. Sol. Cells* **2008**, *92*, 190–193. [CrossRef]

51. Peter, C.; Schmitt, K.; Apitz, M.; Woellenstein, J. Metallo-porphyrin zinc as gas sensitive material for colorimetric gas sensors on planar optical waveguides. *Microsyst. Technol.* **2012**, *18*, 925–930. [CrossRef]

52. Xu, B.; Xu, L.; Gao, G.; Li, Z.; Liu, Y.; Guo, W.; Jia, L. Polyoxometalate-based gasochromic silica. *New J. Chem* **2008**, *32*, 1008–1013. [CrossRef]

53. Wang, Z.; Yuan, X.; Cong, S.; Chen, Z.; Li, Q.; Geng, F.; Zhao, Z. Color-changing microfiber-based multifunctional window screen for capture and visualized monitoring of NH3. *ACS Appl. Mater. Interfaces* **2018**, *10*, 15065–15072. [CrossRef] [PubMed]

54. Shim, G.; Lee, S.Y.; Kalanur, S.S.; Seo, H.J. Eye-readable gasochromic and electrical detectability of hydrogenated Pd-TiO$_2$ to gaseous fluorine species. *Appl. Surf. Sci.* **2018**, *462*, 791–798. [CrossRef]

55. Hakoda, T.; Igarashi, H.; Isozumi, Y.; Yamamoto, S.; Aritani, H.; Yoshikawa, M. Gasochromic property of dehydrogenation-catalyst loaded tungsten trioxide. *J. Phys. Chem. Solids* **2013**, *74*, 200–204. [CrossRef]

56. Okumu, J.; Koerfer, F.; Salinga, C.; Pedersen, T.; Wuttig, M. Gasochromic switching of reactively sputtered molybdenumoxide films: A correlation between film properties and deposition pressure. *Thin Solid Films* **2006**, *515*, 1327–1333. [CrossRef]

57. Deb, S.K. Optical and photoelectric properties and colour centres in thin films of tungsten oxide. *Philos. Mag.* **1973**, *27*, 801–822. [CrossRef]

58. Ito, K.; Ohgami, T. Hydrogen detection based on coloration of anodic tungsten oxide film. *Appl. Phys. Lett.* **1992**, *60*, 938–940. [CrossRef]

59. Krašovec, U.O.; Orel, B.; Georg, A.; Wittwer, V. The gasochromic properties of sol-gel WO$_3$ films with sputtered Pt catalyst. *Sol. Energy* **2000**, *68*, 541–551. [CrossRef]

60. Hemati, M.A.; Ranjbar, M.; Kameli, P.; Salamati, H. Gasochromic tungstenoxide films with PdCl2 solution as an aqueous hydrogen catalyst. *Sol. Energy Mater. Sol. Cells* **2013**, *108*, 105–112. [CrossRef]

61. Salinga, C.; Weis, H.; Wuttig, M. Gasochromic switching of tungsten oxide films: A correlation between film properties and coloration kinetics. *Thin Solid Films* **2002**, *414*, 288–295. [CrossRef]

62. Hsu, W.-C.; Peng, C.-H.; Chang, C.-C. Hydrogen sensing characteristics of an electrodeposited WO$_3$ thin film gasochromic sensor activated by Pt catalyst. *Thin Solid Films* **2007**, *516*, 407–411. [CrossRef]

63. Zayat, M.; Reisfeld, R.; Minti, H.; Orel, B.; Svegl, F. Gasochromic effect in platinum-doped tungsten trioxide films prepared by the sol-gel method. *J. Sol-Gel Sci. Technol.* **1998**, *11*, 161–168. [CrossRef]

64. Orel, B.; Grošelj, N.; Krašovec, U.O.; Ješe, R.A.; Georg, A. IR spectroscopic investigations of gasochromic and electrochromic sol-gel-derived peroxotungstic acid/ormosil composite and crystalline WO$_3$ films. *J. Sol.-Gel. Sci. Technol.* **2002**, *24*, 5–22. [CrossRef]

65. Garavand, N.T.; Mahdavi, S.; Ranjbar, M. The effect of operating temperature on gasochromic properties of amorphous and polycrystalline pulsed laser deposited WO$_3$ films. *Sens. Actuators B Chem.* **2012**, *169*, 284–290. [CrossRef]

66. Ando, M. Recent advances in optochemical sensors for the detection of H$_2$, O$_2$, O$_3$, CO, CO$_2$ and H$_2$O in air. *TrAC Trends Anal. Chem.* **2006**, *25*, 937–948. [CrossRef]

67. Chan, C.-C.; Hsu, W.-C.; Chang, C.-C.; Hsu, C.-S. Hydrogen incorporation in gasochromic coloration of sol–gel WO$_3$ thin films. *Sens. Actuators B Chem.* **2011**, *157*, 504–509. [CrossRef]

68. Chen, H.; Xu, N.; Deng, S.; Lu, D.; Li, Z.; Zhou, J.; Chen, J. Gasochromic effect and relative mechanism of WO$_3$ nanowire films. *Nanotechnology* **2007**, *18*, 205701. [CrossRef]

69. Kalhori, H.; Ranjbar, M.; Salamati, H.; Coey, J. Flower-like nanostructures of WO$_3$: Fabrication and characterization of their in-liquid gasochromic effect. *Sens. Actuators B Chem.* **2016**, *225*, 535–543. [CrossRef]

70. Georg, A.; Graf, W.; Neumann, R.; Wittwer, V. Mechanism of the gasochromic coloration of porous WO$_3$ films. *Solid State Ion.* **2000**, *127*, 319–328. [CrossRef]

71. Yamamoto, S.; Inouye, A.; Yoshikawa, M. Structural and gasochromic properties of epitaxial WO$_3$ films prepared by pulsed laser deposition. *Nucl. Instrum. Methods Phys. Res. B* **2008**, *266*, 802–806. [CrossRef]

72. Behbahani, M.A.; Ranjbar, M.; Kameli, P.; Salamati, H. Hydrogen sensing by wet-gasochromic coloring of PdCl2 (aq)/WO$_3$ and the role of hydrophilicity of tungsten oxide films. *Sens. Actuators B Chem.* **2013**, *188*, 127–136. [CrossRef]

73. Garavand, N.T.; Mahdavi, S. Pt and Pd as catalyst deposited by hydrogen reduction of metal salts on WO$_3$ films for gasochromic application. *Appl. Surf. Sci.* **2013**, *273*, 261–267. [CrossRef]

74. Lee, S.-H.; Cheong, H.M.; Liu, P.; Smith, D.; Tracy, C.E.; Mascarenhas, A.; Pitts, J.R.; Deb, S.K. Raman spectroscopic studies of gasochromic a-WO$_3$ thin films. *J. Electrochim. Acta* **2001**, *46*, 1995–1999. [CrossRef]

75. Lee, Y.-A.; Kalanur, S.S.; Shim, G.; Park, J.; Seo, H. Highly sensitive gasochromic H$_2$ sensing by nano-columnar WO$_3$-Pd films with surface moisture. *Sens. Actuators B Chem.* **2017**, *238*, 111–119. [CrossRef]

76. Shanak, H.; Schmitt, H. Fast coloration in sputtered gasochromic tungsten oxide films. *J. Phys. Status Solidi* **2006**, *203*, 3748–3753. [CrossRef]

77. Nishizawa, K.; Yamada, Y.; Yoshimura, K. Low-temperature chemical fabrication of Pt-WO$_3$ gasochromic switchable films using UV irradiation. *Sol. Energy Mater. Sol.Cells* **2017**, *170*, 21–26. [CrossRef]

78. Kalanur, S.S.; Heo, J.; Yoo, I.-H.; Seo, H. 2-D WO$_3$ decorated with Pd for rapid gasochromic and electrical hydrogen sensing. *Int. J. Hydrogen Energy* **2017**, *42*, 16901–16908. [CrossRef]

79. Zamharir, S.G.; Ranjbar, M.; Salamati, H. Excimer laser treatment of TiO$_2$/WO$_3$ thin films for self-cleaning gasochromic applications: Preparation and characterization. *Sol. Energy Mater. Sol. Cells* **2014**, *130*, 27–35. [CrossRef]

80. Yamaguchi, Y.; Emoto, Y.; Kineri, T.; Fujimoto, M.; Mae, H.; Yasumori, A.; Nishio, K.J. Hydrogen gas-sensing properties of Pt/WO$_3$ thin film in various measurement conditions. *Ionics* **2012**, *18*, 449–453. [CrossRef]

81. Kalanur, S.S.; Yoo, I.-H.; Lee, Y.-A.; Seo, H. Green deposition of Pd nanoparticles on WO$_3$ for optical, electronic and gasochromic hydrogen sensing applications. *Sens. Actuators B Chem.* **2015**, *221*, 411–417. [CrossRef]

82. Kim, J.-H.; Mirzaei, A.; Kim, H.W.; Kim, S.S. Low power-consumption CO gas sensors based on Au-functionalized SnO$_2$-ZnO core-shell nanowires. *Sens. Actuators B Chem.* **2018**, *267*, 597–607. [CrossRef]

83. Chen, S.; Luo, J.; Tan, H.; Chen, J.; Deng, S.; Xu, N. Study of self-heating phenomenon and its resultant effect on ultrafast gasochromic coloration of Pt-WO$_3$ nanowire films. *Sens. Actuators B Chem.* **2012**, *173*, 824–832. [CrossRef]

84. Okazaki, S.; Johjima, S. Temperature dependence and degradation of gasochromic response behavior in hydrogen sensing with Pt/WO$_3$ thin film. *Thin Solid Films* **2014**, *558*, 411–415. [CrossRef]

85. Luo, J.Y.; Deng, S.Z.; Tao, Y.T.; Zhao, F.L.; Zhu, L.F.; Gong, L.; Chen, J.; Xu, N.S. Evidence of localized water molecules and their role in the gasochromic effect of WO$_3$ nanowire films. *J. Phys. Chem. C* **2009**, *113*, 15877–15881. [CrossRef]

86. Luo, J.Y.; Gong, L.; Tan, H.D.; Deng, S.Z.; Xu, N.S.; Zeng, Q.G.; Wang, Y. Study of the catalyst poisoning and reactivation of Pt nanoparticles on the surface of WO$_3$ nanowire in gasochromic coloration. *Sens. Actuators B Chem.* **2012**, *171*, 1117–1124. [CrossRef]

87. Foroushani, F.T.; Tavanai, H.; Ranjbar, M.; Bahrami, H. Fabrication of tungsten oxide nanofibers via electrospinning for gasochromic hydrogen detection. *Sens. Actuators B Chem.* **2018**, *268*, 319–327. [CrossRef]

88. Wisitsoorat, A.; Ahmad, M.; Yaacob, M.; Horpratum, M.; Phakaratkul, D.; Lomas, T.; Tuantranont, A.; Wlodarski, W. Optical H$_2$ sensing properties of vertically aligned Pd/WO$_3$ nanorods thin films deposited via glancing angle rf magnetron sputtering. *Sens. Actuators B Chem.* **2013**, *182*, 795–801. [CrossRef]

89. Chan, C.-C.; Hsu, W.-C.; Chang, C.-C.; Hsu, C.-S. Preparation and characterization of gasochromic Pt/WO$_3$ hydrogen sensor by using the Taguchi design method. *Sens. Actuators B Chem.* **2010**, *145*, 691–697. [CrossRef]

90. Hsu, C.-H.; Chang, C.-C.; Tseng, C.-M.; Chan, C.-C.; Chao, W.-H.; Wu, Y.-R.; Wen, M.-H.; Hsieh, Y.-T.; Wang, Y.-C.; Chen, C.-L. An ultra-fast response gasochromic device for hydrogen gas detection. *Sens. Actuators B Chem.* **2013**, *186*, 193–198. [CrossRef]

91. Chen, M.; Zou, L.; Zhang, Z.; Shen, J.; Li, D.; Zong, Q.; Gao, G.; Wu, G.; Zhang, Z. Tandem gasochromic-Pd-WO$_3$/graphene/Si device for room-temperature high-performance optoelectronic hydrogen sensors. *Carbon* **2018**, *130*, 281–287. [CrossRef]

92. Yamaguchi, Y.; Imamura, S.; Ito, S.; Nishio, K.; Fujimoto, K. Influence of oxygen gas concentration on hydrogen sensing of Pt/WO$_3$ thin film prepared by sol-gel process. *Sens. Actuators B Chem.* **2015**, *216*, 394–401. [CrossRef]

93. Schweiger, D.; Georg, A.; Graf, W.; Wittwer, V. Examination of the kinetics and performance of a catalytically switching (gasochromic) device. *Solar Energy Mater. Solar Cells* **1998**, *54*, 99–108. [CrossRef]

94. Ranjbar, M.N.; Garavand, T.; Mahdavi, S. Electroless plating of palladium on WO$_3$ films for gasochromic applications. *J. Sol. Energy Mater. Sol. Cells* **2010**, *94*, 201–206. [CrossRef]

95. Yamamoto, S.; Takano, K.; Inouye, A.; Yoshikawa, M. Effects of composition and structure on gasochromic coloration of tungsten oxide films investigated with XRD and RBS. *Nucl. Instrum. Methods Phys. Res. B* **2007**, *262*, 29–32. [CrossRef]

96. Hsu, C.-H.; Chang, C.-C.; Yeh, K.-W.; Wu, Y.-R.; Chan, C.-C.; Wang, M.-J.; Wu, M.-K. Pulsed laser deposition of (WO$_3$)1-x (Nb2O5)x thin films: Characterization and gasochromic studies. *Thin Solid Films* **2011**, *520*, 1470–1474. [CrossRef]

97. Ranjbar, M.; Mahdavi, S. Pulsed laser deposition of W-V-O composite films: Preparation, characterization and gasochromic studies. *Sol. Energy Mater. Sol. Cells* **2008**, *92*, 878–883. [CrossRef]

98. Ranjbar, M.; Fardindoost, S.; Mahdavi, A.I. Palladium nanoparticle deposition onto the WO_3 surface through hydrogen reduction of PdCl2: Characterization and gasochromic properties. *Sol. Energy Mater. Sol. Cells* **2011**, *95*, 2335–2340. [CrossRef]

99. Garavand, N.T.; Mahdavi, S. Pd2+ reduction and gasochromic properties of colloidal tungsten oxide nanoparticles synthesized by pulsed laser ablation. *Appl. Phys. A* **2012**, *108*, 401–407. [CrossRef]

100. Li, J.; Zhao, Q.-L.; Zhang, G.-Y.; Chen, J.-Z.; Zhong, L.; Li, L.; Huang, J.; Ma, Z. Synthesis of monoclinic WO_3 nanosphere hydrogen gasochromic film via a sol-gel approach using PS-b-PAA diblock copolymer as template. *Solid State Sci.* **2010**, *12*, 1393–1398. [CrossRef]

101. Li, D.; Wu, G.; Gao, G.; Shen, J.; Huang, F. Ultrafast coloring-bleaching performance of nanoporous WO_3–SiO_2 gasochromic films doped with Pd catalyst. *ACS Appl. Mater. Interfaces* **2011**, *3*, 4573–4579. [CrossRef]

102. Castillero, P.; Rico-Gavira, V.; Lopez-Santos, C.; Barranco, A.; Perez-Dieste, V.; Escudero, C.; Espinós, J.P.; González-Elipe, A.N.R. Formation of subsurface W5+ species in gasochromic Pt/WO_3 thin films exposed to hydrogen. *J. Phys. Chem. C* **2017**, *121*, 5719–15727. [CrossRef]